atmosphere

Article

Exploring the Evolution of Typhoon Lekima (2019) Moving Offshore Northeast of Taiwan with a Multi-Resolution Global Model

Ching-Yuang Huang [1,*], Chau-Hsiang Chang [1] and Hung-Chi Kuo [2]

[1] Department of Atmospheric Sciences, National Central University, Taoyuan City 32001, Taiwan
[2] Department of Atmospheric Sciences, National Taiwan University, Taipei 10617, Taiwan
* Correspondence: hcy@atm.ncu.edu.tw; Tel.: +886-3-4227151 (ext. 65532)

Abstract: Typhoon Lekima occurred in early August 2019 and moved northwestward toward Taiwan. During offshore passage, the typhoon underwent rapid intensification, with a northward deflected track, moving closer to northeastern Taiwan. A global model, MPAS, at a multi-resolution of 60-15-3 km, is utilized with ensemble forecasts to investigate the dynamic processes causing the track deflection and intensity change as well as identify the track uncertainty to initial perturbed conditions under the topographic effects of the Central Mountain Range (CMR). For spinning up the typhoon vortex in ensemble forecasts, dynamic vortex initialization has been enforced with a 3 km resolution targeted at the Taiwan area. As one specific member track is similar to the best track, the track deflection is significantly reduced in the absence of the Taiwan terrain, highlighting the role of the topographic effects of the CMR. For these tracks with similar deflection, the northward deflection is caused by the induced strong flow to the east of the typhoon center in response to the re-circulating flow around southern Taiwan, which produces the wavenumber-one gyre in the asymmetric flow difference to drive the vortex northward. The typhoon translation around the Taiwan terrain is dominated by the changing wavenumber-one horizontal potential vorticity (PV) advection during the track deflection in the ensemble forecasts. The formation of an intense PV tongue along the upper eyewall is a facilitation precondition of RI, while RI can be significantly enhanced in the presence of an intense lower-stratospheric PV core near the upper eye, which is produced by the radial inflow of the developed transverse vortex circulation over the upper-level outflow layer.

Keywords: Typhoon Lekima; MPAS; Taiwan terrain; track deflection; potential vorticity

Citation: Huang, C.-Y.; Chang, C.-H.; Kuo, H.-C. Exploring the Evolution of Typhoon Lekima (2019) Moving Offshore Northeast of Taiwan with a Multi-Resolution Global Model. *Atmosphere* **2022**, *13*, 1817. https://doi.org/10.3390/atmos13111817

Academic Editor: Hisayuki Kubota

Received: 12 September 2022
Accepted: 31 October 2022
Published: 1 November 2022

1. Introduction

Among isolated mesoscale mountains, the Central Mountain Range (CMR) in Taiwan has exerted a great impact on impinging typhoons from different approaching directions. Topographic effects of the CMR on tropical cyclones, as summarized by a review article by Wu and Kuo [1], have significantly affected cyclone tracks, in addition to the enhanced local rainfall over Taiwan. The induced rainfall amounts associated with the tropical cyclones and intense typhoons impinging on Taiwan are closely modulated by both tracks and the moving speeds of the typhoons ([2]). The tracks basically dictate the geometric distributions of the major rainfall, while the duration of the cyclone at various translational speeds highly correlates with rainfall production. Understanding the variability of the typhoon tracks near or around the Taiwan terrain appears to be vital to the forecast impacts but remains quite limited due to a great variety of translational cyclones.

In the past, a number of numerical studies have investigated the track variations associated with approaching cyclones/typhoons in response to the topographic effects of the CMR or similar idealized terrain (e.g., [3–26]). A cyclonic curvature path of the westbound cyclone that passed the northern portion of a CMR-like terrain has been identified, which leads to a northward turning before landfalling at or passing around northern Taiwan

([3,5]). The approaching westbound cyclones may be still deflected slightly northward upstream, but can be significantly southward near landfall at the central-northern portion of the CMR or idealized CMR-like terrain (e.g., [7,14,15,17,18,20]). It has been well understood that such a southward turning of a westbound cyclone is attributed to the channeling effects of northerly flow ahead of the mountain base as well as the mid-tropospheric flow acceleration over the terrain ([15,18]).

It is crucial to identify the track responses of tropical cyclones moving toward a mesoscale mountain in terms of a dynamic view. For westbound cyclones past a mesoscale mountain range, the upstream track deflection has been related to the dominant factor R/L_y regarded as a nondimensional vortex size with R (the radius of maximum tangential wind of the upstream vortex) and L_y (the mountain length scale in the direction normal to the vortex movement). For a small value of R/L_y, an intense westbound cyclone will tend to be deflected southward when moving to the central or southern portion of the idealized terrain ([18,20]). When R/L_y becomes smaller, stronger terrain blocking will be induced ahead of the steep slope and thus leads to a rapid southward turning in response to the intensified northerly wind west of the vortex center. However, the upstream track of such westbound or northwest bound cyclones may get deflected northward ahead of the terrain as close to the southern portion of the terrain (e.g., [17]).

The track behaviors of observed west-northwestward or northwestward typhoons moving toward Taiwan have exhibited some northward deflection, moving offshore closer to northern Taiwan, and were exhibited in Maria (2018) and Lekima (2019), respectively ([24,25]). We have identified twelve typhoons in the past 70 years moving westward to northwestward offshore near northern Taiwan with northward track deflection—Grace (1958), Cora (1966), Betty (1972), Nelson (1985), Fred (1994), Rananim (2004), Masta (2005), Wipha (2007), Trami (2013), Maria (2018), Lekima (2019) and Hagupit (2020). These deflected tracks possibly possess similar deflection mechanisms as illustrated in [25,26], where the recirculation flow of the typhoon vortex around the southern island plays a vital role. The nondimensional control parameter of R/L_y has to be revised by using the projected mountain length (L_E, the effective terrain scale perpendicular to basic flow) to replace L_y to explain the favorable northward turning ([25]). The northward track deflection for both typhoons is in response to the enhanced wind east of the typhoon center when the recirculating flow over the southern end of Taiwan converges with the inner vortex east of Taiwan. The induced stronger asymmetric southerly wind east of the inner vortex will drive the typhoon vortex northward. Thus, the increase in the nondimensional vortex size reduces the effect of mountain blocking to prevent the track from a southward turn near the terrain base.

The northward track deflection of both west-northwestward Maria and northwestward Lekima has been reasonably captured by the 7 km resolution of the CWB global model FV3GFS ([24,25]). It is particularly interesting to find that both typhoon tracks indeed are somewhat sensitive to the resolved typhoon structure for which the forecasts are affected by physics parameterizations used by the model. However, the northward track can be induced when the simulated upstream tracks are close to the steering direction in spite of some deviations in typhoon intensity. Several important questions immediately arise: Will the typhoon track and intensification be sensitive to perturbed initial conditions? How are both related to dynamic processes in the typhoon vortex? Can the topographic effects of the CMR cause the northward track deflection to be identified in the general forecasts with those perturbed initial conditions? These questions stimulate the motivation of this study but focus on the northwestward Lekima that exhibits a larger northward track deflection than the west-northwestward Maria due to a reduced size of L_E for the former. Moreover, the former exhibits stronger intensification and intensity near the track deflection than the latter.

In this study, we will apply a multi-resolution global model, the Model for Prediction Across Scales-Atmosphere (MPAS-A, hereafter MPAS) to simulate Lekima for understanding the predictability of the track deflection and the dynamic processes involved in the

typhoon movement and intensification. As shown in Figure 1, the use of an enhanced resolution zone of 3 km in the MPAS, targeted in the vicinity of Taiwan, would help resolve the high mountain terrain and the incoming typhoon, as shown in simulations of Typhoon Nesat (2017) landfalling at northern Taiwan ([21]) and Tropical Cyclone Atsani (2020) passing around southern Taiwan ([26]). For spinning up the initial typhoon vortex, dynamic vortex initialization (DVI) ([23]) has been applied in the numerical experiment. Ensemble forecasts to expose the impacts of initial uncertainty are produced by adding small random perturbations to the initial conditions with the spin-up vortex. We have analyzed the angular momentum budget and potential vorticity budget to explain the typhoon intensification and track deflection. The DVI and diagnostics of the PV budget have been incorporated into the multi-resolution MPAS developed for typhoon forecasts in the vicinity of the CMR. The above developed framework facilitates use of the MPAS in this study to complement the previous work with CWB FV3GFS.

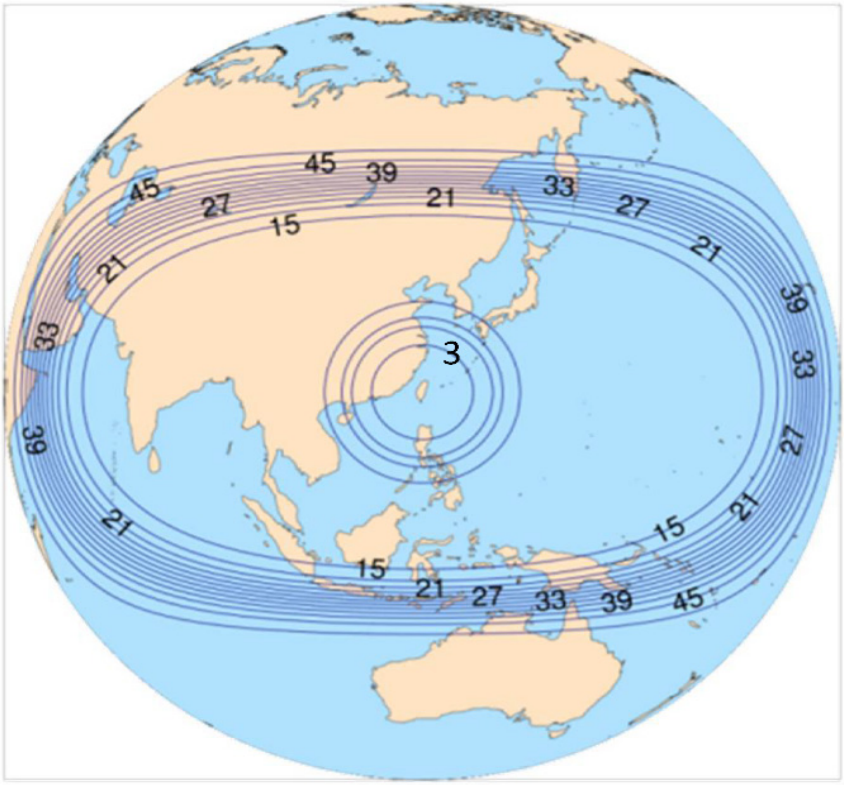

Figure 1. The approximate mesh resolution of MPAS-60-15-3 km indicated by the contours at an interval of 3 km.

We briefly describe the MPAS model and its default physics schemes in Section 2, together with the introduction of the numerical experiments and Typhoon Lekima. The simulation results of the numerical experiments are presented and discussed in Section 3. The budget analyses from the simulation results are provided in Section 4 to aid an interpretation of the track responses and intensification of Lekima. Finally, conclusions are given in Section 5.

2. The Model and Experiments

2.1. The MPAS

The global model used in this study is the MPAS-Atmosphere Version 6.1 mainly developed at NCAR (Boulder, CO, USA) ([27]). The MPAS adopts an unstructured centroidal Voronoi mesh so that variable horizontal resolution that gradually increases toward some specific region of interest can be applied to enhance the resolvable details of the flow as well

as the topography. The use of a 60-15-3 km variable-resolution mesh for the MPAS has been successfully applied to simulate northwest-bound typhoons passing Taiwan ([21–23]). The highest 3 km resolution region in that study, as shown in Figure 1, is centered over Taiwan and covers the paths of impinging typhoons from different directions. For convenience in application, MPAS defaults have collected two suites of physics schemes, the mesoscale-reference suite and the convection-permitting suite (the M-suite and C-suite, respectively), both combining different physical parameterization schemes. Based on the simulation results for sixteen typhoons in 2015–2020, the M-suite has somewhat outperformed the C-suite in track prediction ([23]).

For all the experiments in this study, the model initial conditions take the first guess from the National Center for Environmental Prediction (NCEP) Global Data Assimilation System (GDAS) Final (FNL) operational global analysis (0.25° × 0.25°). The MPAS has set a default of a total of 41 vertical levels with a model top at 30 km height. The sea surface temperature (SST) obtained from the GDAS dataset is kept unchanged during the MPAS forecasts.

2.2. Vortex Initialization

It is often required to reinitialize the model's initial state obtained from the global dataset such as GDAS for improving the intensity and structure of the initial typhoon vortex which is usually relatively weaker than that from the best track data. We have developed a DVI scheme that conducts continuously cycled integration of 1 h for cycle runs with the forecast model to match the intensity of the model typhoon vortex with the best track data, either on the minimum sea-level pressure (MSLP) or maximum wind speed of the vortex near the surface (hereafter V_{max}), called P-match or V-match, respectively ([23]). After each cycle, only the 1 h forecasted vortex within a radius of 600 km from the vortex center at the arrival position is reallocated to the best track position, that is the departure position of the vortex at the initial time, and then replaces the departing vortex. It is more complicated to relocate the arrival vortex and replace the departing vortex over the unstructured grids of the MPAS than the uniform grids of WRF ([26]). The methodology of the DVI may refer to Huang et al. [23]. Application of the DVI has been shown to greatly improve both intensity and track forecasts of typhoons over the Western North Pacific (WNP) (e.g., [23,26]).

2.3. Lekima and Numerical Experiments

Lekima formed east of the northern Philippines over the WNP and was categorized as a tropical storm at 0000 UTC on 4 August 2019 by the Japan Meteorological Agency (JMA). During the northwestward movement toward northern Taiwan, Lekima quickly intensified as a moderate typhoon on 7 August, and became an intense typhoon at 0830 UTC on 8 August and reached the peak intensity of 910 hPa (central sea-level pressure) and 53 m s^{-1} (maximum wind speed) at 1200 UTC on 8 August from the report of Central Weather Bureau in Taiwan. Rapid intensification (RI) develops from 1800 UTC on 6 August to 0600 UTC on 8 August as the typhoon's maximum wind speed exceeds 30 knots/24 h or 42 hPa/24 h defined by Kaplan and DeMaria (2003) ([28]). The RI occurrence of Lekima has been attributed to the storm passage over the warm SST larger than 30 °C under relatively lower vertical wind shear in this region ([29,30]). During the intensity evolution, Lekima underwent an eyewall replacement cycle with the formation of the concentric eyewall as found in other intense typhoons ([31]). The mechanism of RI associated with the double-warm core structure of Lekima in the tropospheric vortex was investigated using a regional model by Shi and Chen (2021) ([30]).

In this study, MPAS experiments with the 60-15-3 km resolution are conducted for Lekima. The forecasts are focused on the initial time of 1200 UTC on 6 August prior to the track deflection. The model takes the NCEP global FNL data (0.25° by 0.25°) as the first guesses for the initial conditions. The initial vortex of Lekima from the global analysis is somewhat relatively weaker than the observed. We thus apply the DVI to spin up the vortex following ([23]). In the DVI, the mesoscale-reference physics schemes are used

with the V-match where the cycled integration will be stopped when the simulated V_{max} matches or has exceeded the best track value. For spreading the initial environmental conditions, the DVI results from this experiment (denoted as the CTL experiment) are randomly perturbed by RANDOMCV of WRF DA (see https://www2.mmm.ucar.edu/wrf/users/docs/user_guide_v4 (accessed on 25 January 2019) to generate twenty ensemble members (denoted as M1–M20). These perturbations are essentially small at a Gaussian distribution of the ensemble and are added to all prognostic model variables based on the background errors for the summer time All the experiment forecasts are conducted with the MPAS 60-15-3 km mesh for integration of a total of 120 h. The model forecasts have used physics schemes including the cumulus parameterization of Grell–Freitas, the cloud microphysics of Thompson, the surface model of Noah, the planetary boundary parameterization of YSU, the surface-layer similarity of Monin-Obukhov as well as the longwave and shortwave radiation of RRTMG. For references of these physics schemes, please refer to Huang et al. ([23]). For comparisons, some experiments have reset the Taiwan terrain heights to zero to explore the impacts of the topographic effect of the CMR on typhoon evolution.

3. Simulation Results

3.1. Track and Intensity Simulations with Taiwan Terrain

Figure 2 shows the simulated tracks and intensities of the ensemble members (M1–M20) and CTL. Most of the tracks tend to exhibit a larger spreading after the observed northward deflection and deviate to the north at later stages (Figure 2a). While some of the tracks may follow the best track, most of the tracks actually are displayed more southward. The CTL shows that the northward deflection is consistent with the observation, despite that it deviates northward to the north of Taiwan at later stages. Such track behaviors of CTL are quite similar to those using the global FV3 model with a 7 km resolution ([25]).

With the V-match in DVI, all the experiments exactly capture the initial V_{max} but with slightly deeper MSLP compared to the best track values. Consequently, most of the simulated typhoon intensities follow the best track intensities quite well in the first 30 h but are somewhat underpredicted for the peak values in 48–54 h of the forecasts. Larger deviations with overpredicted intensity are evident at later stages and can be attributed to their associated larger track errors, most of which prevent the simulated typhoon from an observed landfall in China. Except for one outlier, all the experiments produce a pressure drop from 972 to 940 hPa in the earlier 24 h. On the other hand, most V_{max} values increase from the initial intensity of 30 m s^{-1} to over 40 m s^{-1}, but are still below 45 m s^{-1}, within the same time. Thus, the DVI helps approximate the observed RI. By applying a similar DVI for Lekima's simulations with the 2 km resolution, a RI pattern is also captured ([30]). We will be more concerned with the simulation results by 60 h with reasonable track and intensity forecasts.

3.2. Typhoon Simulations with and without the Taiwan Terrain

Among M1–M20, several experiments show pronounced track deflection at earlier stages and are selected for comparison. For these experiments and the CTL experiment, we have conducted their terrain-sensitivity experiments where the Taiwan terrain heights are reset to zero. Figure 3 shows the simulated tracks and intensities for the selected M3, M6, and M9 as well as CTL with and without the terrain. For the four experiments, removal of the terrain height has resulted in largely reduced track deflection, especially for CTL. Indeed, the a northward track deflection may not be induced as seen in some of M1-20 when a track is present too closer to Taiwan (see Figure 2a). The track becomes even southward when the simulated vortex is more southward and moves toward northern Taiwan. This is consistent with the finding ([24]) that the track deflection is more pronounced only when the upstream track is close to the observed track. CTL with and without the Taiwan terrain produces slightly stronger earlier intensification in both V_{max} and MSLP on the first day,

comparable to the best track intensity. However, neither of the four experiments can well capture the intensification on the second day and the observed peak intensity at 48 h.

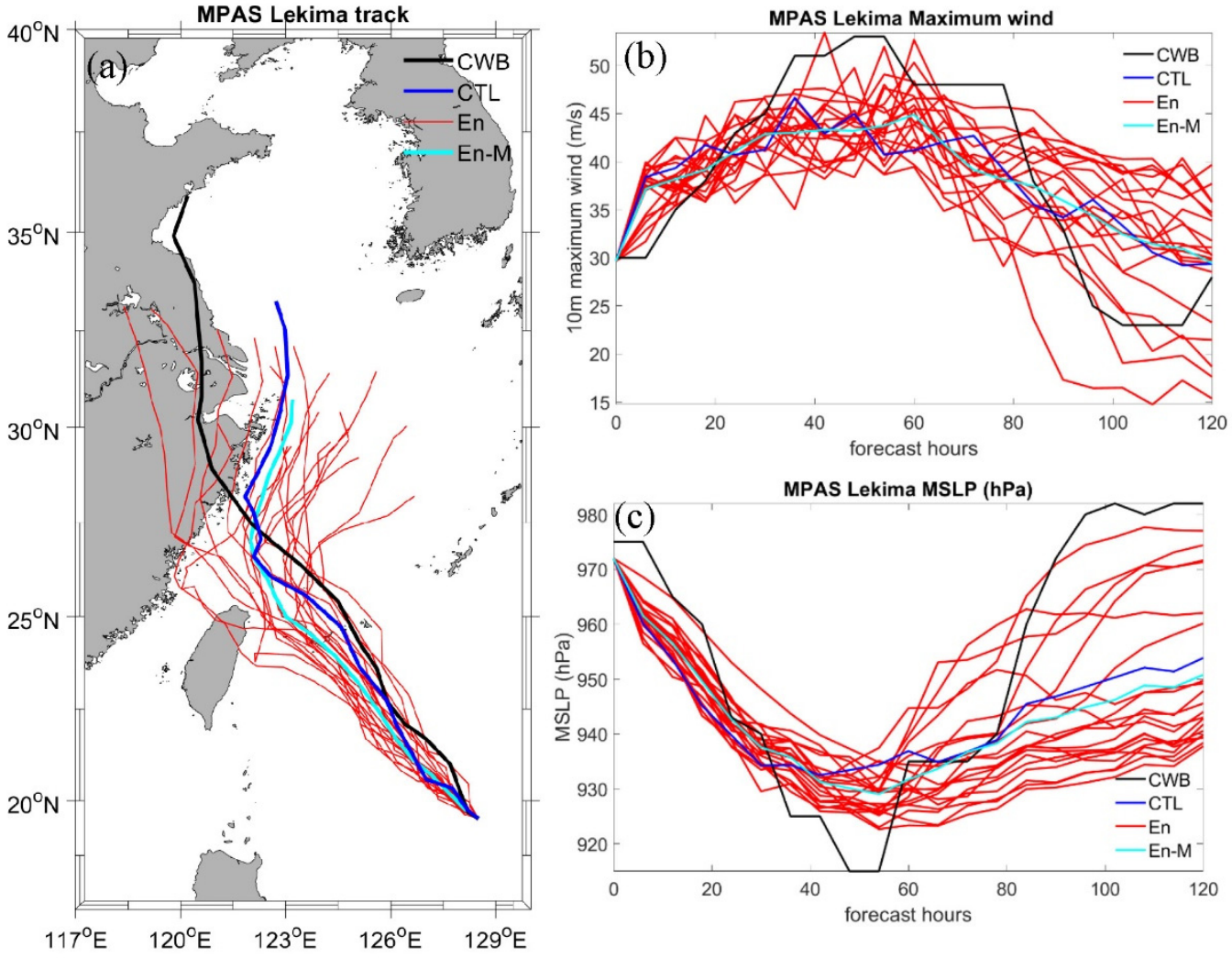

Figure 2. (**a**) Ensemble tracks of M1–M20 (red), ensemble mean (purple), CTL (blue) and the best track from CWB (black). (**b**) as in (**a**) for the maximum wind speed of the typhoon at 10 m height. (**c**) as in (**b**) but for minim sea-level pressure.

3.3. Forecast Sensitivity to Physical Parameterizations

We have also conducted physics-sensitivity tests for the four experiments that produce northward track deflection. Their simulation results are shown in Figure 4. As the cumulus parameterization scheme is changed from Grell–Freitas to the new Tiedtke, all four experiments can produce stronger MSLP throughout the forecasts. On the other hand, the typhoon intensity is somewhat weakened when the cloud microphysics scheme is changed from Thompson to WSM6. For CTL, the use of the new Tiedtke has produced a stronger RI than the observed before the track deflection, but with a more westward-deviated track. Northward track deflection appears to be induced for all the sensitivity tests, in spite of large differences in their vortex intensities. This is speculated as the impacts of similar clustering tracks of the four experiments (see Figure 2).

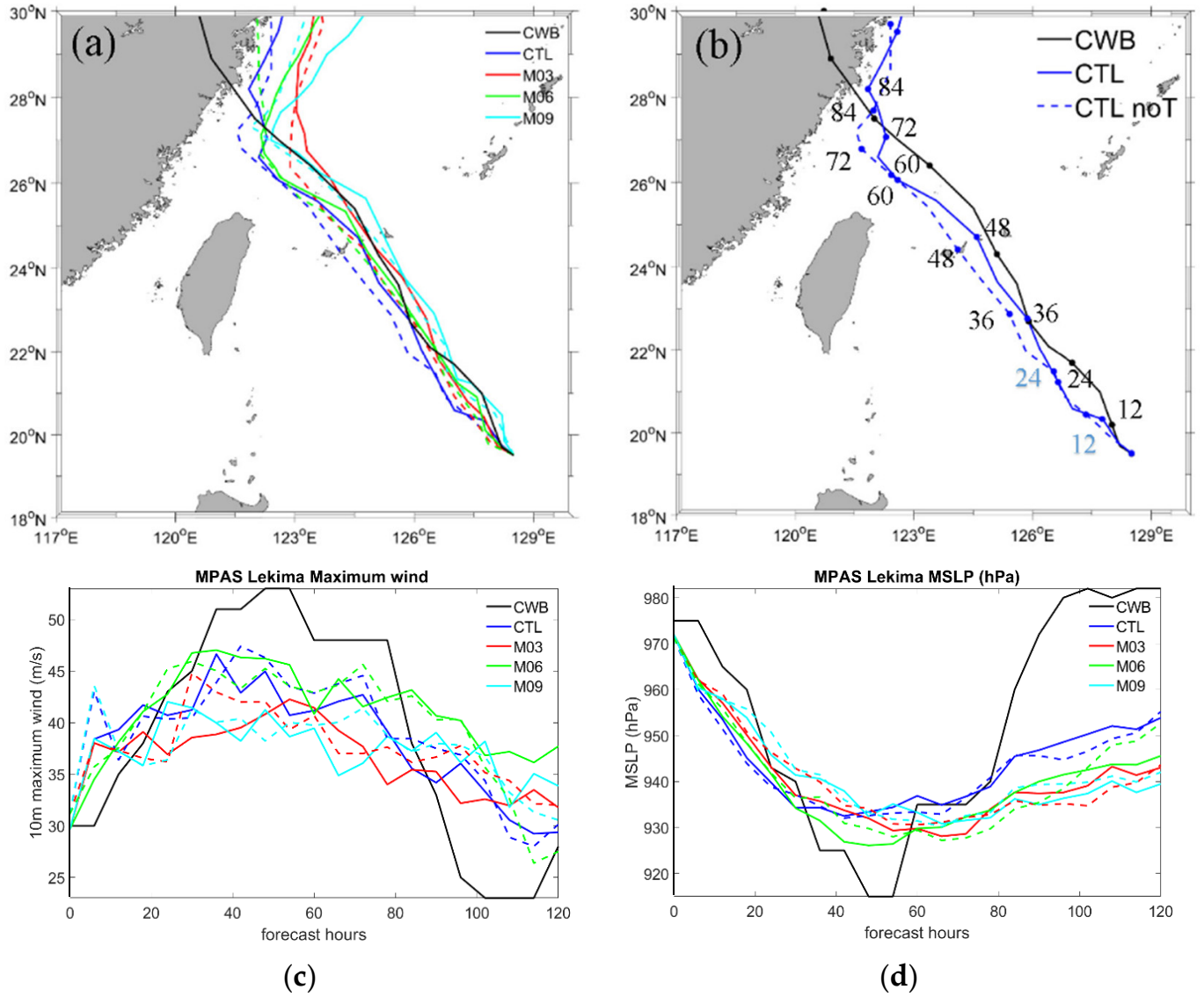

Figure 3. (**a**) The tracks (solid) of CTL (blue), M3 (red), M6 (orange), and M9 (purple) and their experiments without the Taiwan terrain (dashed), with the CWB best track (black) included. (**b**) as in (**a**) but for CTL (solid blue) and its sensitivity experiment without the Taiwan terrain (dashed blue) with the labeled numbers for forecast hours. (**c**,**d**) as in (**a**) but for the maximum wind speed (m s^{-1}) of the typhoon at 10 m height and minimum sea-level pressure (hPa), respectively.

Note that the strongest typhoon intensification in the first 40 h presented for the sensitivity test of CTL has exceeded the observed RI of Lekima, where the central sea-level pressure has deepened from 972 to 920 hPa in 30 h in Figure 4b and the V_{max} has intensified from 30 to 58 m s^{-1} during the same period (not shown). RI may be regarded as severe RI far exceeding the typical RI threshold of 30 knots/24 h.

3.4. Typhoon Circulation

Figure 5 shows the simulated typhoon circulation at 850 hPa at 1800 UTC on 8 August (54 h of forecast) for CTL M6 and M9; M3 is similar to M9 and thus is not shown. This is about the time that the simulated Lekima takes the largest track deflection associated with significant asymmetric development. For CTL, Taiwan's terrain has blocked the typhoon circulation to the east of Taiwan and southwest of the vortex center. The flow southeast of the vortex center is stronger in the presence of Taiwan terrain, which facilitates a more northward track. Such enhanced asymmetric wind also occurs in M6 and M9. Indeed, all

the four experiments show the same wind enhancement in the SE quadrant of the vortex that originates from the recirculating flow of the typhoon passing around the southern end of Taiwan as found in Huang et al. (2022) ([25]). These results indicate a general role of Taiwan's terrain in modulating the asymmetric typhoon circulation to change steering.

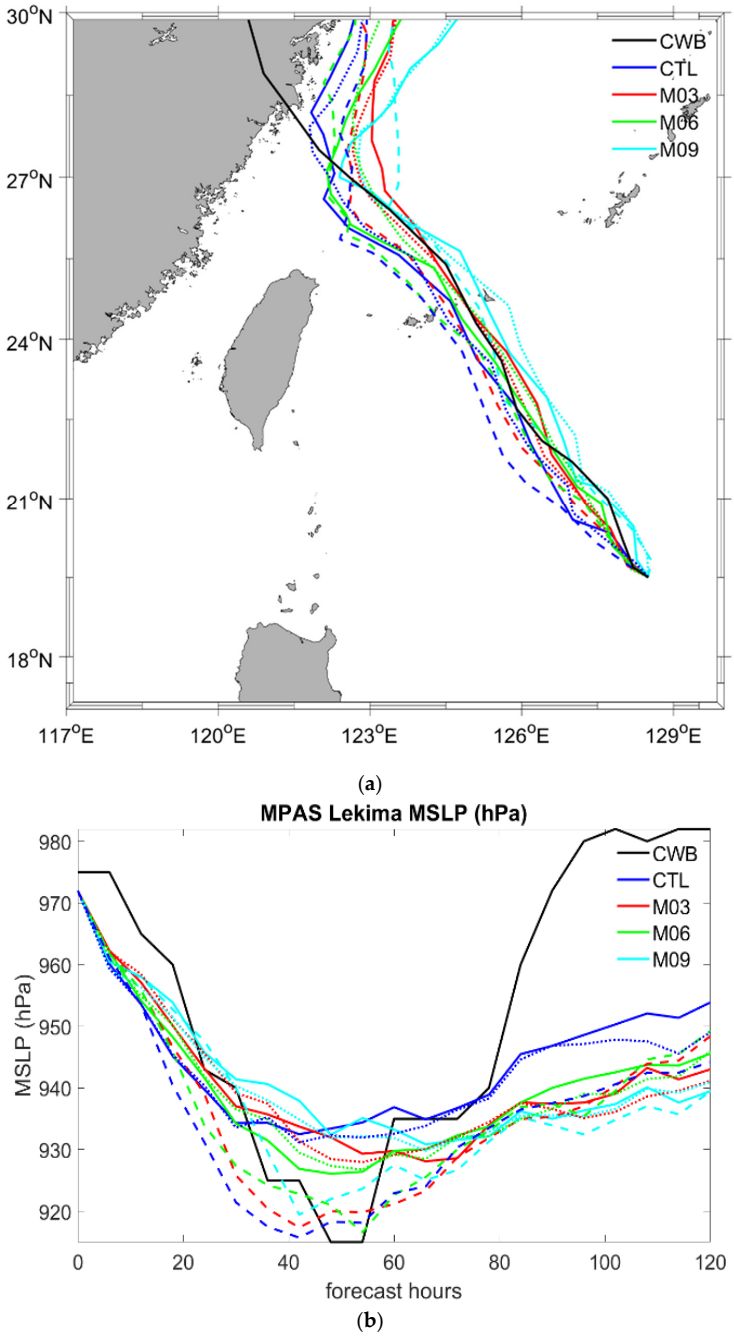

Figure 4. (**a**) The CWB best track (black) and the simulated tracks (solid) of M3 (red), M6 (orange), M9 (purple), and CTL (blue) as well as their physics-sensitivity experiments in which the Grell–Freitas cumulus scheme is changed to the new Tiedtke scheme (dashed) and the cloud microphysics Thompson scheme is changed to the WSM6 scheme (dotted). (**b**) in (**a**) but for the evolution of the minimum sea-level pressure (hPa) of the typhoon.

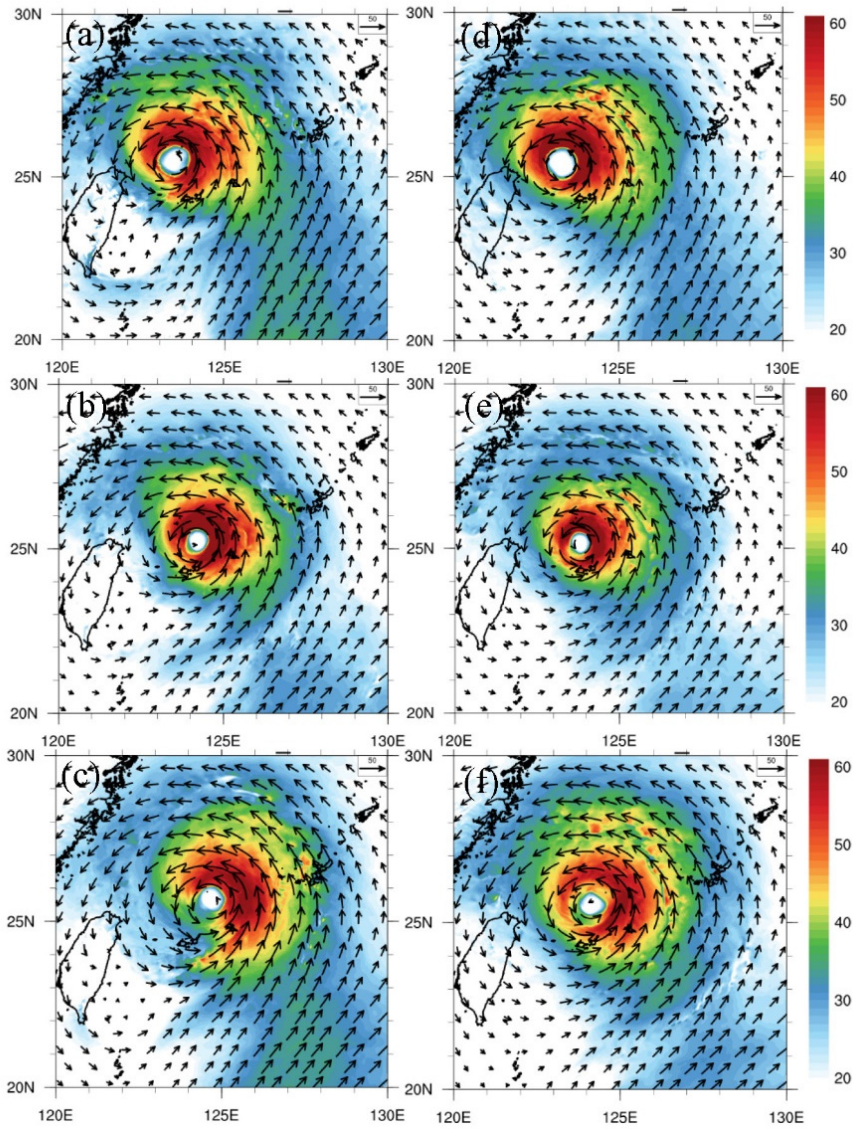

Figure 5. The simulated typhoon circulation at 850 hPa at 1800 UTC 8 August (54 h of forecast) for (**a**) CTL and (**d**) as in (**a**) but without the Taiwan terrain. (**b**) and (**e**) as in (**a**) and (**d**), respectively, but for M6. (**c**) and (**f**) as in (**a**) and (**d**), respectively, but for M9.

3.5. Evolution of the Vortex Wind Speed

To further identify the impacts of the vortex wind enhancement, we examine the evolution of the low-level wind speed for the four experiments as shown in Figure 6. The simulated wind speed inside the radius of 150 km from the vortex center and in the vertical of 0–2 km height is averaged. In the vertical axis indicating the forecast time, stronger vortex wind commences to northeast-southeast (45–135 degrees) earlier from the incipient time, but becomes significantly enhanced after 0000 UTC on 8 August for M3, M6, and M9, and even in advance near 1200 UTC on 7 August for CTL associated with the largest track deflection. The larger wind speed to the northeast of the vortex is corresponding to the northwestward steering of Lekima. Indeed, significant wind enhancement occurs closer to the east (90 degrees) after 1800 UTC on 7 August (30 h of forecast) for CTL, and is somewhat delayed for the other three experiments. The temporal variations of the stronger vortex core for the four experiments are related to the magnitude and occurrence time of their track deflection, but all show the topographic effects of the Taiwan terrain on the asymmetric wind development of the vortex.

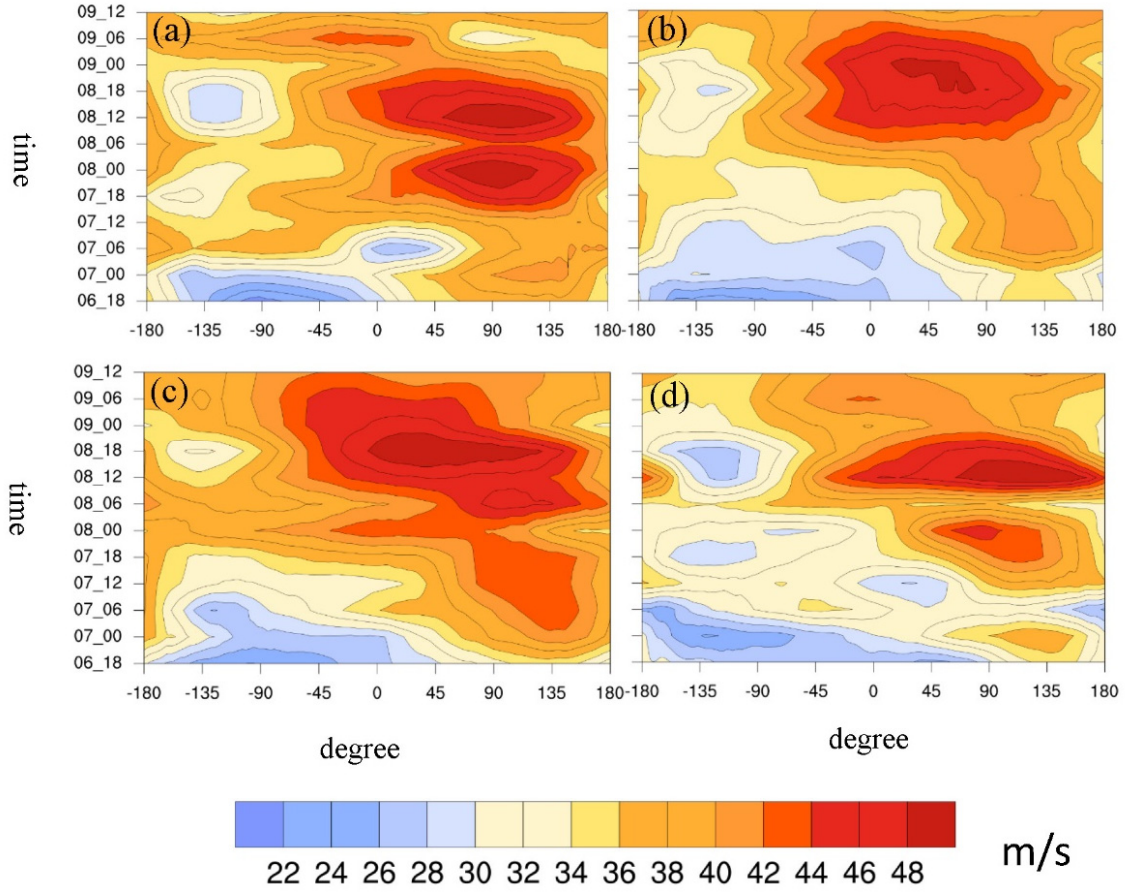

Figure 6. The evolution of the wind speed (shaded colors at an interval of 2 m s^{-1}) averaged within the radius of 150 km of the vortex center and in 0–2 km height during the forecast for (**a**) CTL, (**b**) M3, (**c**) M6, and (**d**) M9. In the horizontal axis, 0, 90 and 135 degrees indicate the north, east, and southeast, respectively.

3.6. The Asymmetric Flow Affecting Tracks

The track deflection of the simulated Lekima is closely related to the development of enhanced asymmetric wind for the four experiments (CTL, M3, M6, and M9). Figure 7 shows the wind differences (averaged in about 850–700 hPa) between the wavenumber-one flow of the experiments with and without the Taiwan terrain at the times when the track deflection begins at 0600 UTC 8, 1800 UTC 8, 1800 UTC 8, and 1200 UTC 8 and completes at 1800 UTC 8, 0600 UTC 9, 0000 UTC 9, and 0000 UTC 9 for CTL, M3, M6, and M9, respectively. Near the track deflection, there are pronounced northerly and southerly wind differences east and southwest of the inner vortex, respectively. It is constituted by a pair of large gyres providing the westerly-northerly flow crossing the vortex core, which facilitates the vortex to move accordingly. Despite the detailed differences between the four experiments, these gyres tend to rotate counterclockwise so that more easterly flow can penetrate into the vortex core when the track becomes more westward after the deflection. The results are similar to the idealized simulation of Tang and Chan ([17]) and the same case simulation of Huang et al. ([25]). In this study, the four experiments are not unique to the presence of the northward track defection of Lekima.

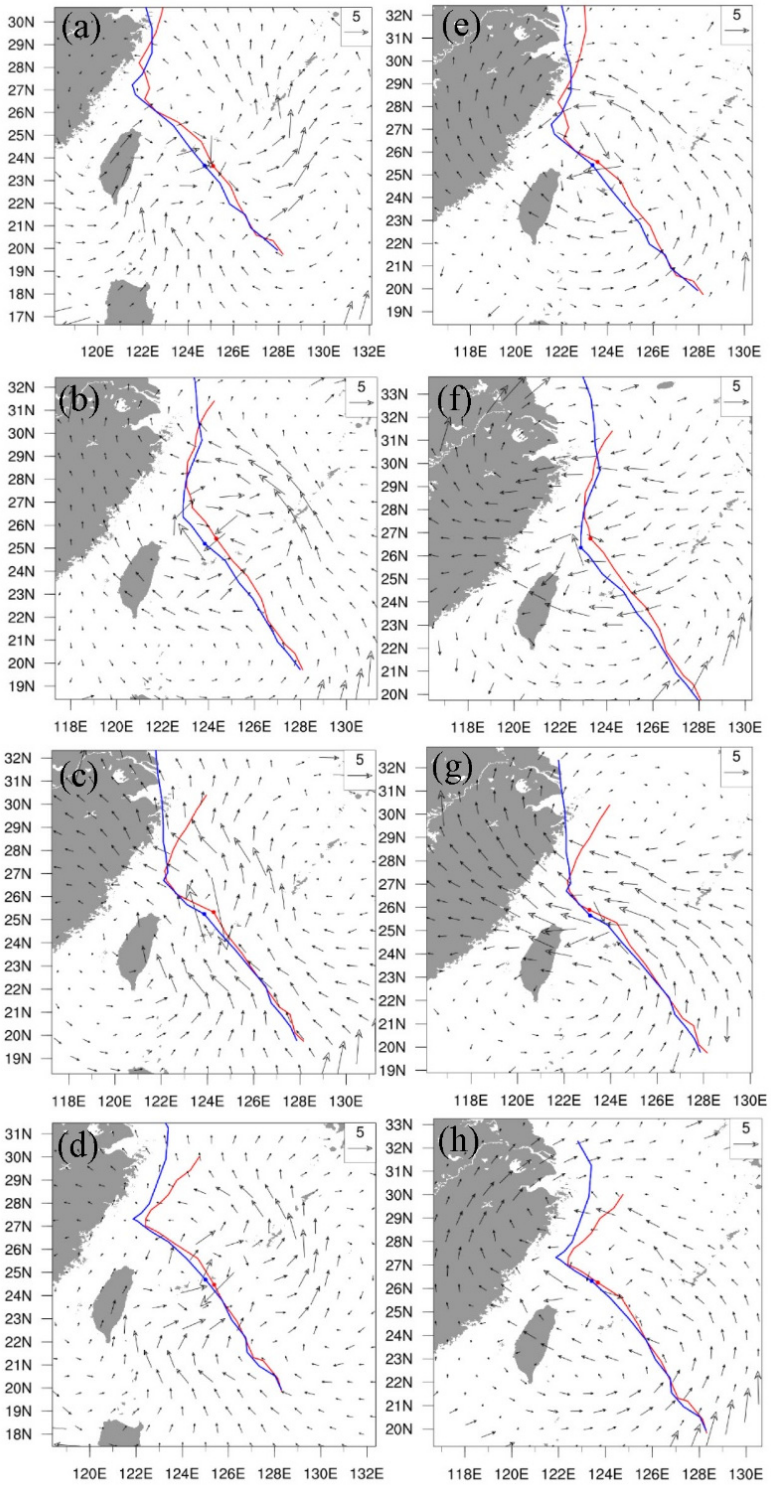

Figure 7. The wind differences (averaged in about 850–700 hPa) between the wavenumber-one flow of the experiment with and without the Taiwan terrain for CTL, M3, M6, and M9 at the times when the track deflection begins at (**a**) 0600 UTC 8 for CTL, (**b**) 1800 UTC 8 for M3, (**c**) 1800 UTC 8 for M6, and (**d**) 1200 UTC 8 for M9 and completes at (**e**) 1800 UTC 8 for CTL, (**f**) 0600 UTC 9 for M3, (**g**) 0000 UTC 9 for M6, and (**h**) 0000 UTC 9 for M9, respectively. In all panels, a reference vector (m s^{-1}) is given at the upper right and the simulated tracks with and without the Taiwan terrain are overlapped in red and blue lines, respectively.

4. Discussion

As shown in the previous section, the CTL experiment has illustrated the features of typhoon circulation with reasonable intensity and the most pronounced track deflection. We will provide some investigations for CTL regarding the dynamic processes in typhoon evolution based on diagnostics of angular momentum (AM) budget and potential vorticity (PV) budget. The flow is decomposed to obtain the mean (symmetric) and eddy (asymmetric) parts for calculating both AM budget and PV budget. Formulations of the azimuthal-mean AM budget and the wavenumber-one PV budget are given by Huang et al. (2020) ([24]) and Nguyen and Huang (2021) ([32]), respectively. For both budgets, the turbulent diffusion is neglected as the flow above the inflow boundary layer is more concerned with the steering of the typhoon.

4.1. Azimuthal-Mean Angular Momentum Budget

Figure 8 shows the height-radius cross-sectional azimuthal mean of angular momentum budget (m^2 s^{-2}) for CTL at 0600 UTC on 8 August (42 h of forecast). Both radial advection and vertical advection of mean AM produce comparable major negative and positive contributions (Figure 8a,b) that appear to counteract each other. Larger AM is being transported away from the eyewall by the radial advection of the outflow, but is mainly compensated by the vertical AM transport of the eyewall updraft. As the tangential wind speed at the lower levels decreases outward from the central eyewall and upward near the top of the near-surface inflow as shown in Huang et al. (2020) ([24]), radial advection of mean AM is positive and vertical advection of mean AM is negative below 1.5 km height. In the eyewall, radial advection of asymmetric eddy AM (Figure 8c) is mostly negative and is somewhat compensated by positive vertical advection of asymmetric eddy AM (Figure 8d). The impacts of the Coriolis force are contributing to positive and negative AM tendencies in the boundary layer and upper outflow layer, respectively, as a consequence of the strong near-surface inflow and upper outflow (Figure 8e). As a sum (without the turbulent friction term), the net AM budget (Figure 8f) is mainly negative in the eyewall and low-level outer vortex at this time near the track deflection as seen in the ceased intensification (see Figure 3d). The overall features are similar to those in the simulations of Maria ([24]), except that the near-surface AM tendency is positive for the latter. Indeed, we find that the net AM budget above the inflow boundary layer does not commonly provide similar AM tendencies of the typhoon near the track deflection for all four experiments, despite that their most significant positive and negative terms remain the same. Removal of the Taiwan terrain has also somewhat modified the AM budget terms for the four experiments but still retains the same major contributions. The intensity and structure variations of the inner vortex do not greatly affect the track evolution as found in the physics-sensitivity tests.

Figure 9 shows the height-radius cross-sectional azimuthal mean of angular momentum budget (m^2 s^{-2}) for CTL at 1800 UTC on 8 August (54 h of forecast) as the track deflection is near completion. The major negative and positive budget terms remain unchanged, both still counteracting each other (Figure 9a,b). However, radial advection of asymmetric eddy AM becomes more negative in the outer lower-tropospheric vortex (Figure 8c), while its associated vertical advection (Figure 8d) remains to produce some positive tendency in the eyewall below 9 km height. At 54 h, the tropospheric AM tendency is mainly negative outside the eyewall as the typhoon has further weakened (see Figure 3). The AM budget terms for the four experiments are more similar at this time, but M3, M6, and M9 produce less negative AM tendency in the inner tropospheric vortex (not shown) than CTL shown in Figure 9f. Thus, the vortex eddy becomes more important at later deflection stages to consume the mean AM due to the development of a more asymmetric vortex.

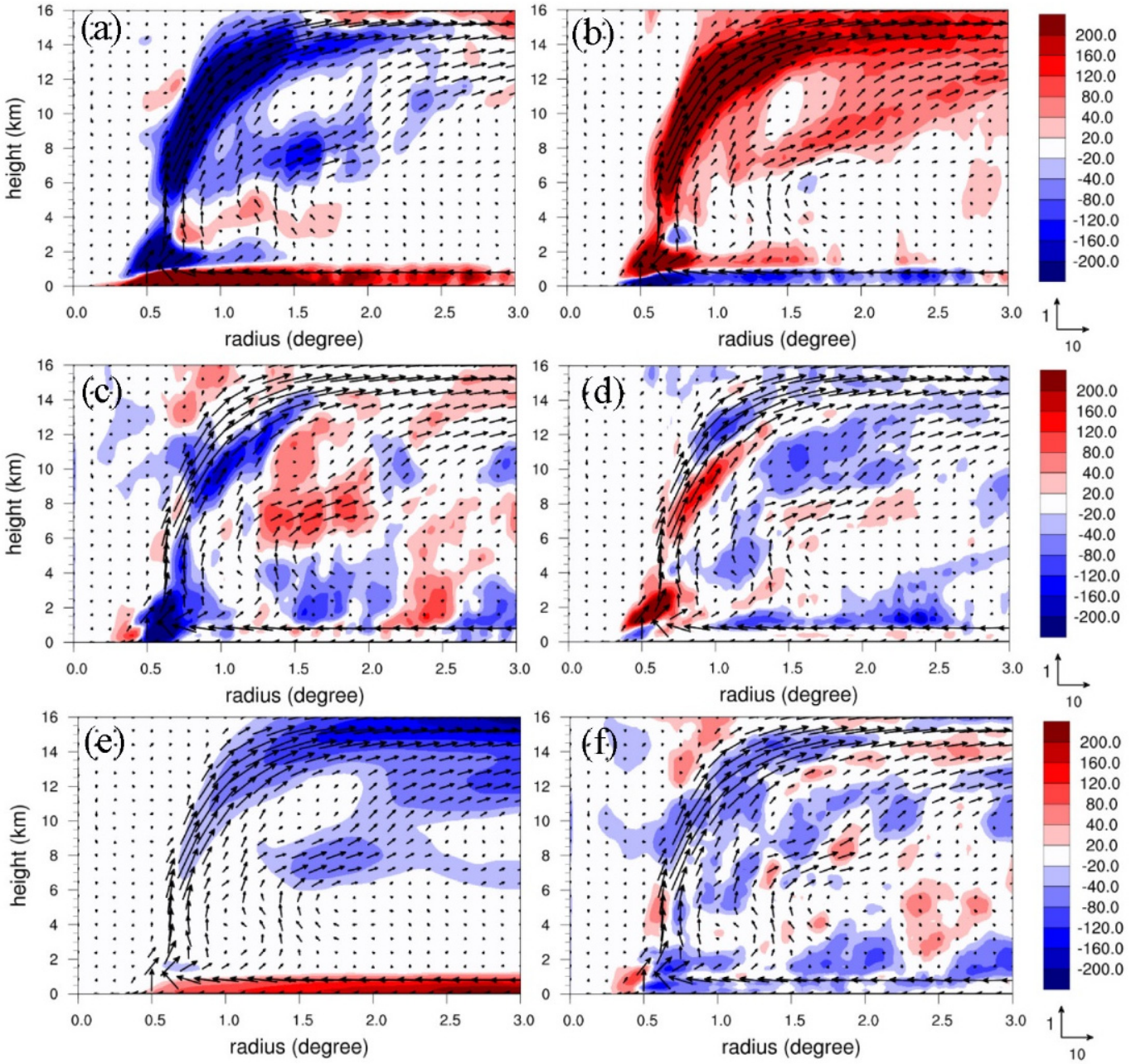

Figure 8. The height-radius cross-sectional azimuthal mean of angular momentum budget ($m^2\ s^{-2}$) for CTL at 0600 UTC on 8 August including (**a**) radial advection of mean AM, (**b**) vertical advection of mean AM, (**c**) radial advection of asymmetric eddy AM, (**d**) vertical advection of asymmetric eddy AM, (**e**) the torque exerted by the Coriolis force, and (**f**) the sum of all the budget terms. The horizontal radial and vertical wind components are referenced to the vectors ($m\ s^{-1}$) at the lower right for all the panels.

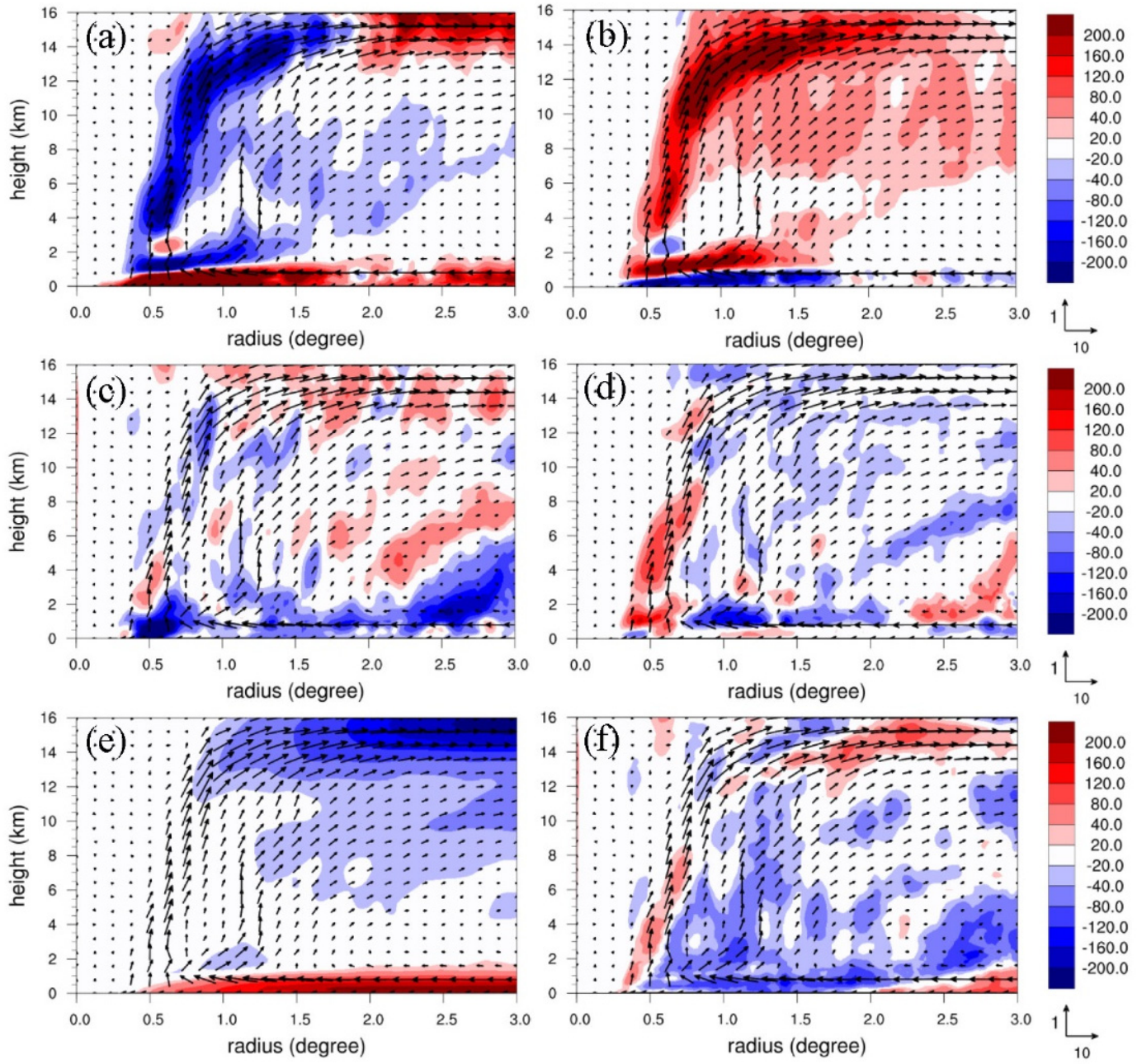

Figure 9. As in Figure 8 but for CTL at 1800 UTC on 8 August (54 h of forecast). The horizontal radial and vertical wind components are referenced to the vectors (m s^{-1}) at the lower right.

4.2. Potential Vorticity Budget

A potential vorticity budget can be used to diagnose the vortex motion that is steered toward the maximum positive PV tendency. We have applied the regression method to estimate the simulation translation of Lekima following Wu and Wang (1999) ([33]). This method has shown a reasonable quantification for the typhoon translation induced by different physical processes in Huang et al. (2019) ([21]). In this study, the regression takes into account the wavenumber-one (WN-1) PV budget within a radius of 150 km of the vortex center. Figure 10 shows the WN-1 horizontal flow and PV tendency budget averaged in 1–8 km height and within 30 min of the analysis time of 0600 UTC on 8 August for CTL. At this time near the track deflection, the net WN-1 PV budget (Figure 10a) is more dominated by horizontal PV advection (Figure 10b) with induced northward translation of 2.7 m s^{-1} compared to vertical PV advection with induced northward translation of

1.37 m s^{-1} (Figure 10c) and differential diabatic heating with induced northward translation of 0.38 m s^{-1} (Figure 10d). The induced total translation is mainly northward at a speed of 4.43 m s^{-1}, which follows the embedded WN-1 flow quite well and is in good agreement with the actual movement at 42 h as shown in Figure 3.

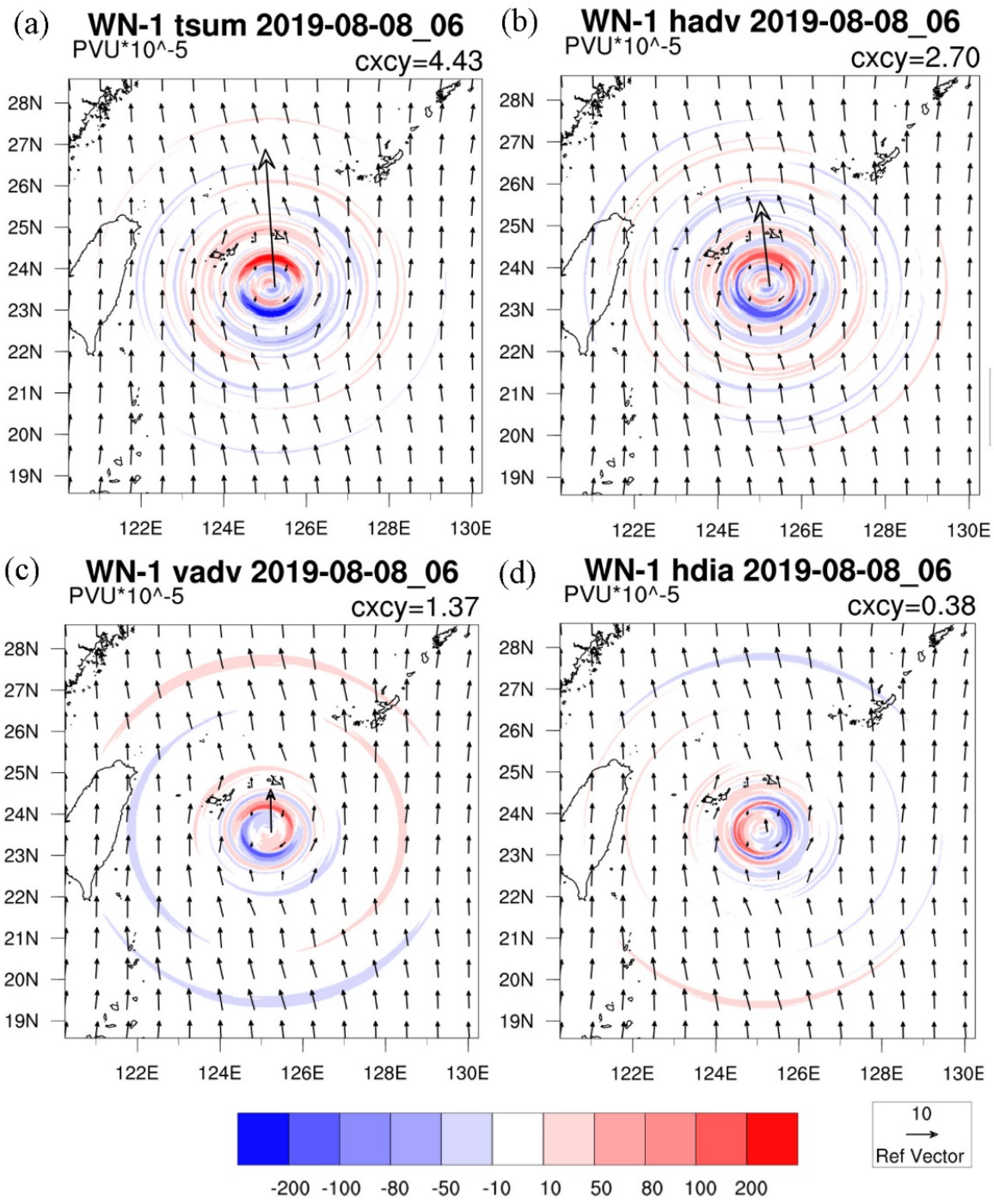

Figure 10. Wavenumber-one (WN-1) horizontal flow and PV tendency budget (shaded colors in 10^{-5} PVU s^{-1} with the reference bar below) averaged in 1–8 km height and in 30 min of the analysis time at 0600 UTC 8 August for CTL. The budget terms are (**a**) net budget, (**b**) horizontal PV advection, (**c**) vertical PV advection, and (**d**) differential diabatic heating. The WN-1 horizontal wind (m s^{-1}) is referenced to the vector at the lower right. The number at the top right of each panel indicates the magnitude of the regressed translation speed of the vortex corresponding to the vector given at the center of each panel (typhoon center).

Figure 11 shows the PV budget results, similar to Figure 10, but at the analysis time of 1800 UTC on 8 August (54 h of forecast) for CTL when the track deflection is near completion. At this time, the actual vortex movement is somewhat westward. The induced total translation of 3.95 m s^{-1} is roughly north-northwestward (Figure 11a), which is also dominated by horizontal PV advection with an induced north-northward translation of 3.83 m s^{-1} (Figure 11b) considerably larger than both vertical PV advection and differential diabatic heating (Figure 11c,d). The WN-1 flow embedded around the inner vortex is roughly northwestward, but mainly northward further northwest and southeast of the vortex. Consequently, the vortex moves roughly northwestward at this time as seen in Figure 3. For the vortex translating into the open ocean away from the topography, the vortex movement is dominated by the horizontal flow as found in Huang et al. (2022) ([26]) and Nguyen and Huang (2021) ([32]).

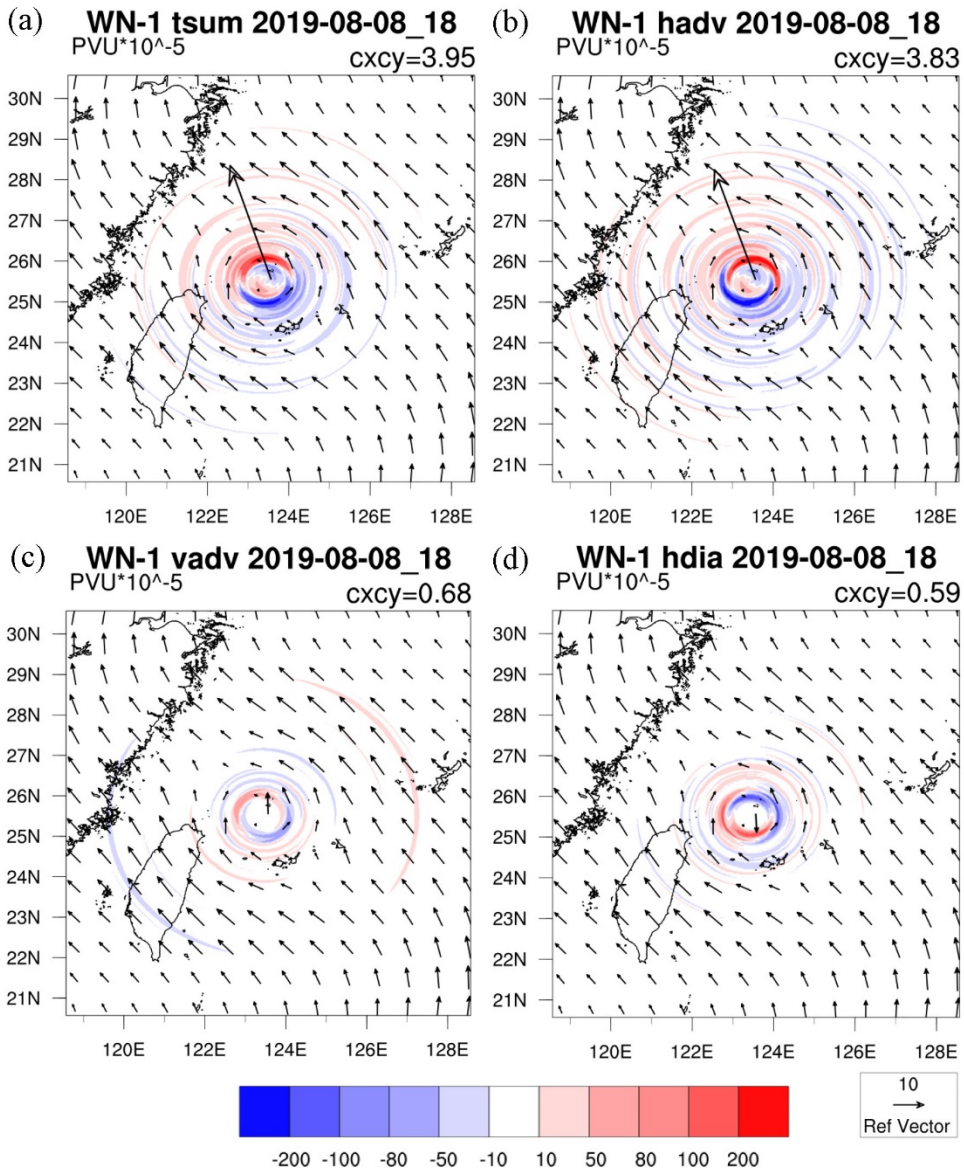

Figure 11. As in Figure 10 but for the analysis time of 1800 UTC 8 August (54 h of forecast) for CTL.

4.3. Typhoon Translation with Perturbed Initial Conditions

In this subsection, we summarize the impacts of different perturbed initial conditions on typhoon translation and track deflection by utilizing the WN-1 PV budget. Figure 12 shows the vortex translation induced by different wavenumber-one PV budget terms for

CTL, M3, M6, and M9, and their sensitivity experiments without the Taiwan terrain. In general, the net PV budget is dominated by horizontal PV advection near the deflection and after its completion (42–60 h). At 66 h, as the typhoon moves close to mainland China, this dominance is less pronounced. All four experiments show similar translation directions with time but at somewhat different speeds. Comparing their track behaviors as shown in Figure 7, the typhoon movement actually differs with time. For example, the track for CTL begins to turn more westward at 48 h from northward at 42 h as seen in Figure 3, which is well captured by the net WN-1 PV tendency (Figure 12a). The track for M3 is mainly northward in 48–54 h and is also reflected in the net PV tendency (Figure 12b). However, it becomes more westward after 54 h for M6 and slower after 48 h for M9, and both are also well indicated by the net PV tendency. Nevertheless, some northward translation near and after the track deflection is commonly produced for the four experiments.

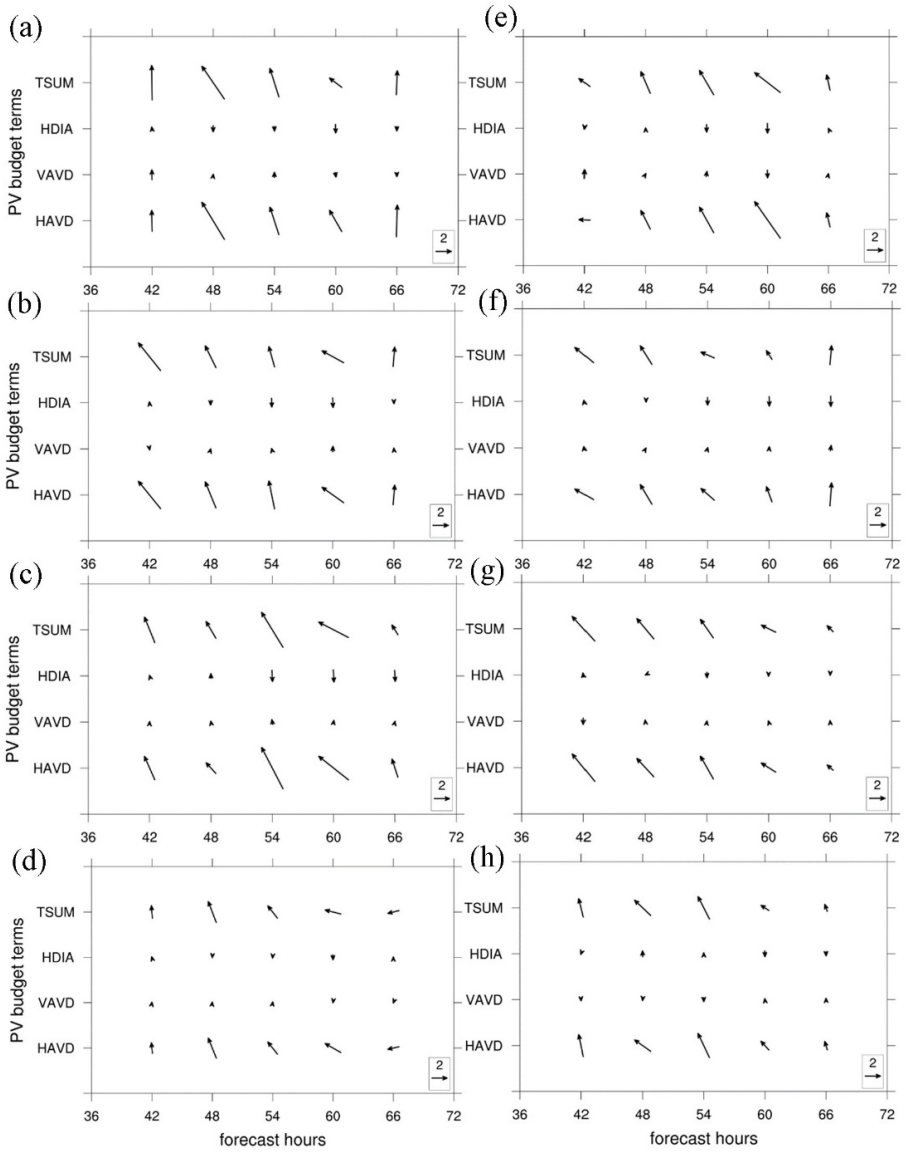

Figure 12. The translation vectors induced different wavenumber-one PV budget terms including the net budget (TSUM), differential diabatic heating (HDIA), vertical PV advection (VDAD), and vertical PV advection (HAVD at different forecast times (hours) for (**a**) CTL, (**b**) M3, (**c**) M6, and (**d**) M9. (**e**–**h**), as in (**a**–**d**), respectively, but without the Taiwan terrain. The translation vectors are referenced to the vector (m s^{-1}) given at the lower right of each panel.

The track behaviors can be modified when the Taiwan terrain is removed. For CTL, the net PV tendency without the impact of the Taiwan terrain indicates much less northward movement and slower translation before 54 h (Figure 12e). In general, the vortex movement for M3 and M6 is slower and less northward as seen in their net PV tendencies (Figure 12f,g). However, the difference is less pronounced for M9 as the deviations between the tracks with and without the Taiwan terrain are smaller and appear at later stages (see Figure 7d,h). After 54 h, the former is more westward than the latter as found in their net PV budget (Figure 12d,h). Note that the former track for M6 indeed becomes more westward near the later deflection (see Figure 7c), which might be contributed by the effect of differential diabatic heating that induces a southward translation of about 2 m s^{-1} in the presence of the Taiwan terrain. However, horizontal PV advection remains to dominate the vortex movement with and without the Taiwan terrain.

4.4. Rapid Intensification Facilitated by Lower-Stratospheric Responses

The simulated intensification of Lekima is changed by different physics schemes as shown in Figure 4. The use of the new Tiedtke cumulus parameterization has considerably increased the intensification rate within the second forecast day, in particular for CTL. The central sea-level pressure dropping larger than 50 hPa in the earlier 30 h has exceeded the typical RI. The typhoon intensification is dynamically linked with the evolution of the total PV amount in the inner vortex as illustrated in Huang et al. (2022) ([23]). Figure 13 shows the azimuthal-mean PV at 42 and 54 h for CTL and its sensitivity test with the new Tiedtke scheme at 30 and 42 h. At 42 h, there are major PV zones located at the lower-stratospheric layer over 16 km height, the upper eye in 12–16 km height, and the tropospheric eyewall below 12 km height (Figure 13a). The formation of the intense PV tongue extended from the upper tropospheric eyewall is a precondition signature of typical RI as shown in Tsujino and Kuo (2020) ([34]). At 54 h, the typhoon intensity for CTL has decreased in association with the reduced PV amounts inside 0.5 degrees and an outward displacement of the eyewall (Figure 13b). These results at early stages with a typical RI are consistent with previous studies for RI (e.g., [30,34,35]).

A stronger RI can be produced in the sensitivity experiment with the new Tiedtke for CTL. At 30 h, the major PV features associated with this sensitivity experiment are similar to those at 42 h for CTL (Figure 13c). However, the lower-stratospheric PV (LSPV) above 16 km height has significantly intensified with the lowest central sea-level pressure of 920 hPa at this time. Above the upper outflow at about 13–18 km height, a radial inflow actually is induced to transport the LSPV into the region of the upper eye. An intense LSPV core exceeding 60 PVU can be produced near the upper eye. A strong downward connection of LSPV with the tropospheric PV is also evident inside the radius of the maximum wind speed of the vortex (R_{max}). At 42 h, the typhoon intensity slightly declined with the major PV features (Figure 13d) similar to CTL at 54 h. There is a difference of about 15 hPa in the central sea-level pressure between the two experiments (see Figure 4), but their PV intensities and structures in the inner vortex are only slightly different. Thus, the formation of the intense LSPV core near the upper eye is a signal of enhanced RI when the LSPV is being produced inside R_{max} by the developing transverse vortex circulation over the intense upper outflow layer. Similar lower-stratospheric PV and transverse circulation are also exhibited in the Lekima simulation of Shi and Chen (2021) using a regional model ([30]). Herein, the significance of the LSPV core formation in facilitating the enhanced RI in Lekima is highlighted by the MPAS simulations in this study. It is noted that the LSPV signal as a facilitation precondition of RI for Lekima also appears in other super-intense typhoons associated with severe RI that will be reported in another study.

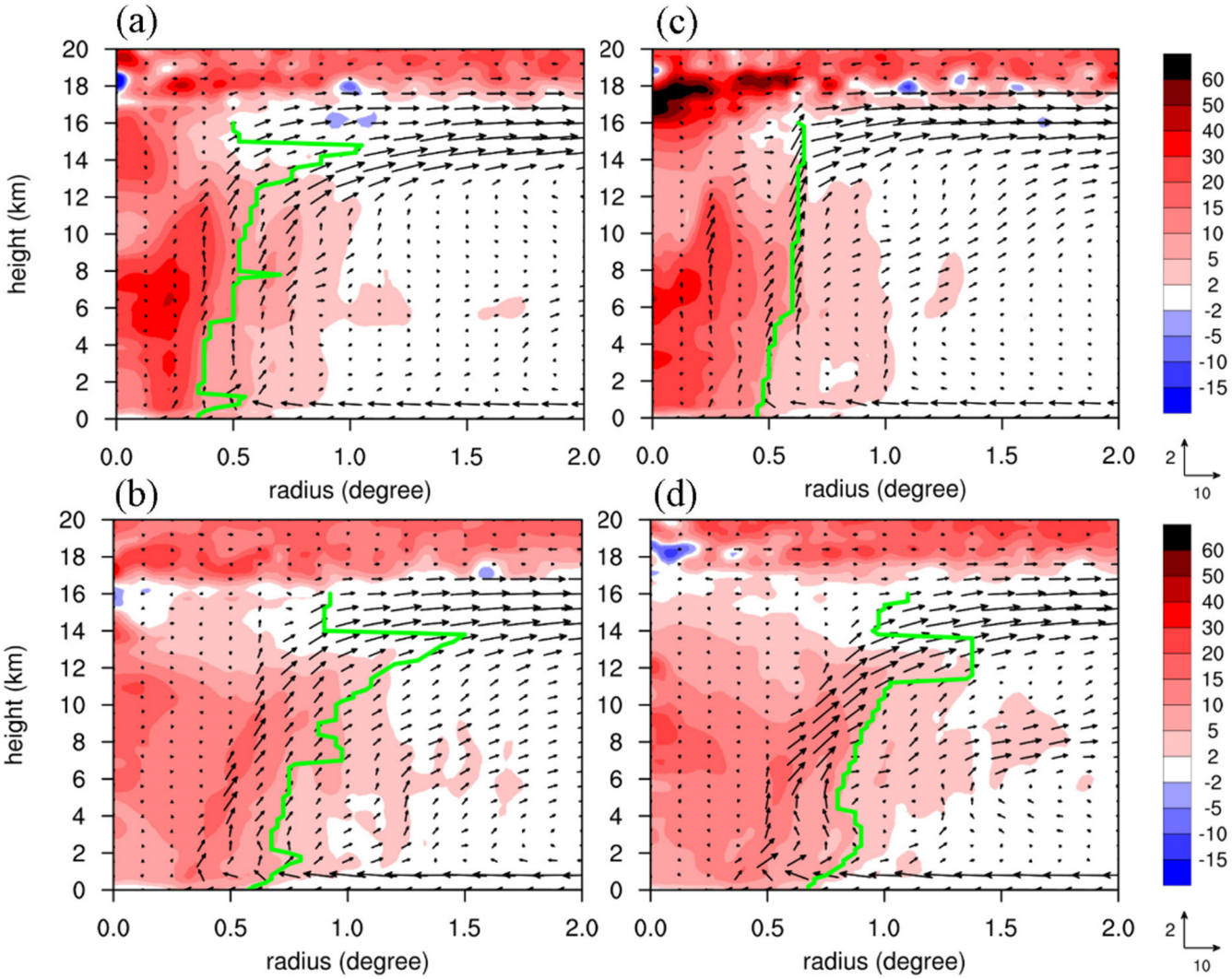

Figure 13. (**a**) The height-radius cross-sectional potential vorticity (shaded colors in PVU) at 42 h for CTL, (**b**) as in (**a**) but at 54 h. (**c**) as in (**a**) but at 30 h for the sensitivity experiment where the Grell–Freitas cumulus scheme in CTL is changed to the new Tiedtke scheme, and (**d**) as in (**c**) but at 42 h. The horizontal radial and vertical wind components are referenced to the vector (m s^{-1}) given at the lower right. The bold green line in each panel indicates the radius of maximum horizontal wind speed.

5. Conclusions

Typhoon Lekima, occurring early August 2019, moved northwestward toward Taiwan and took a northward-deflecting track offshore northeast of Taiwan. Before the earlier track deflection, rapid intensification took place with a central sea-level pressure deepening of 70 hPa in 40 h. In this study, a global model MPAS at a multi-resolution of 60-15-3 km, with a 3 km resolution targeted at the Taiwan area, is utilized to explore the track responses of Lekima and identify the topographic effects of the CMR on the typhoon and the associated track deflection. A dynamic vortex initialization (DVI) is applied to spin up the inner vortex core, which employs a continuously cycled model integration of 1 h for a number of runs until the integrated vortex has reached the observed best track maximum wind speed of the vortex. For forecast sensitivities to initial conditions, twenty members are generated by randomly perturbing the initial model state with the spin-up vortex.

The ensemble forecasts of twenty members have collected a sufficient spreading of simulated typhoon tracks, but with similar maximum intensities. All the members produce similar typhoon intensification rates, but only approximate the observed RI at the

early stage. Some of the cyclone tracks have been reasonably simulated with northward track deflection. We selected four forecasts with more pronounced track deflection more consistent with the best track. Terrain-sensitivity tests for the four experiments, which reset the Taiwan terrain heights to zero, show that the northward track deflection is not produced, but associated with similar intensification rates and peak intensities for the four members. The northward track deflection induced by the topographic effect of the Taiwan terrain is similar to that explored in Huang et al. ([25]) that the northerly flow component east of the vortex center is enhanced by the joined recirculating flow of the typhoon around the southern end of Taiwan to drive the vortex northward. This track deflection mechanism is further illustrated by the four members in this study. A common feature of their differences in wavenumber-one flow exhibits a pair of large gyres around the typhoon center near the earlier deflection, which then rotates counterclockwise with time following the continued deflection. The wavenumber-one potential vorticity budget for these ensemble forecasts indicates that the vortex motion is dominated by horizontal PV advection, while both vertical PV advection and differential diabatic heating are only minor. This can be attributed to the fact that the inner typhoon core is moving offshore and away from the Taiwan terrain.

The angular momentum (AM) budget near the track deflection indicates that the rotational momentum of the inner typhoon is mainly contributed by negative AM tendency from radial advection of mean AM and positive AM tendency from vertical advection of mean AM, both appearing to counteract each other. Radial advection of asymmetric eddy AM is also negative in the eyewall but somewhat compensated by positive vertical advection of asymmetric eddy AM. After the track deflection is completed, the typhoon intensity is weakened in the control experiment, owing to the increased negative impacts from the radial advection of both mean and eddy AM in the more-asymmetric lower-tropospheric vortex.

The typhoon intensification and peak intensity are affected by physical parameterizations in the forecasts, but without greatly reducing the track deflection. Some specific cumulus schemes may produce the strongest RI and intensity, close to the best track values. The evolution of the vortex intensification is closely linked with the intensity of azimuthal-mean PV in the inner vortex. A typical RI can be approximately induced when the tropospheric PV tongue in the upper eyewall is produced as a facilitation precondition of RI ([34]). As the tropospheric PV in the inner vortex is decaying, the developed typhoon circulation also gradually weakens. However, for a RI to be enhanced at earlier development stages, a lower-stratospheric PV (LSPV) core near the upper eye needs to be generated through the developed transverse vortex circulation. For Lekima, a strong downward connection of LSPV with the upper-tropospheric PV in the inner vortex is evident during the enhancement of RI. The mechanisms of enhanced RI associated with other super-intense typhoons have also been investigated and the results will be presented in another study.

This study has largely complemented our previous FV3GFS simulations ([25]) by investigating the forecast track sensitivities to the initial perturbations in a spin-up vortex for Typhoon Lekima (2019) and detailing the AM budget and PV budget for the associated track deflection mechanism from the ensemble. Both high-resolution MPAS and FV3GFS simulations show similar track deflection of Lekima in response to the topographic effects of the Taiwan terrain. This study further explores the track behaviors and dynamics from the ensemble forecasts to identify that the track deflection of Lekima is probably not induced. The RI signature of the simulated Lekima regarding the induced intense LSPV core has also been highlighted in this study.

Author Contributions: Conceptualization, C.-Y.H.; methodology, C.-Y.H.; software, C.-H.C.; formal analysis, C.-Y.H. and C.-H.C.; data curation, C.-H.C.; writing—original draft preparation, C.-Y.H.; writing—review and editing, C.-Y.H. and H.-C.K.; project administration, C.-Y.H. All authors have read and agreed to the published version of the manuscript.

Funding: This study was supported by the Ministry of Science and Technology (MOST) (grant No. MOST 110-2111-M-008-014) in Taiwan.

Institutional Review Board Statement: Not applicable.

Informed Consent Statement: Not applicable.

Data Availability Statement: The best track data are obtained from the CWB in Taiwan and the model forecasts are available from the workstation of the typhoon laboratory at the Department of Atmospheric Sciences, National Central University in Taiwan from 140.115.35.103.

Acknowledgments: Thi-Chinh Nguyen helped on editing the manuscript. We are thankful for National Center for High-performance Computing (NCHC) in Taiwan for providing computational and storage resources.

Conflicts of Interest: The authors declare no conflict of interest.

References

1. Wu, C.-C.; Kuo, Y.-H. Typhoons affecting Taiwan: Current understanding and future challenges. *Bull. Am. Meteorol. Soc.* **1999**, *80*, 67–80. [CrossRef]
2. Hsu, L.-H.; Kuo, H.-C.; Fovell, R.G. On the geographic asymmetry of typhoon translation speed across the mountainous island of Taiwan. *J. Atmos. Sci.* **2013**, *70*, 1006–1022. [CrossRef]
3. Chang, W.-J. The orographic effects induced by an island mountain range on propagating tropical cyclones. *Mon. Weather Rev.* **1982**, *110*, 1255–1270. [CrossRef]
4. Bender, M.A.; Tuleya, R.E.; Kurihara, Y. A numerical study of the effect of island terrain on tropical cyclones. *Mon. Weather Rev.* **1987**, *115*, 130–155. [CrossRef]
5. Yeh, T.-C.; Elsberry, R.L. Interaction of typhoons with the Taiwan orography. Part I: Upstream track deflections. *Mon. Weather Rev.* **1993**, *121*, 3193–3212. [CrossRef]
6. Yeh, T.-C.; Elsberry, R.L. Interaction of typhoons with the Taiwan orography. Part II: Continuous and discontinuous tracks across the island. *Mon. Weather Rev.* **1993**, *121*, 3213–3233. [CrossRef]
7. Lin, Y.-L.; Han, J.; Hamilton, D.W.; Huang, C.-Y. Orographic influence on a drifting cyclone. *J. Atmos. Sci.* **1999**, *56*, 534–562. [CrossRef]
8. Kuo, H.-C.; Williams, R.; Chen, J.-H.; Chen, Y.-L. Topographic effects on barotropic vortex motion: No mean flow. *J. Atmos. Sci.* **2001**, *58*, 1310–1327. [CrossRef]
9. Lin, Y.-L.; Ensley, D.B.; Chiao, S.; Huang, C.-Y. Orographic influences on rainfall and track deflection associated with the passage of a tropical cyclone. *Mon. Weather Rev.* **2002**, *130*, 2929–2950. [CrossRef]
10. Lin, Y.-L.; Chen, S.-Y.; Hill, C.M.; Huang, C.-Y. Control parameters for the influence of a mesoscale mountain range on cyclone track continuity and deflection. *J. Atmos. Sci.* **2005**, *62*, 1849–1866. [CrossRef]
11. Huang, C.-Y.; Lin, Y.-L. The influence of mesoscale mountains on vortex tracks: Shallow-water modeling study. *Meteorol. Atmos. Phys.* **2008**, *101*, 1–20. [CrossRef]
12. Jian, G.-J.; Wu, C.-C. A numerical study of the track deflection of Supertyphoon Haitang (2005) prior to its landfall in Taiwan. *Mon. Weather Rev.* **2008**, *136*, 598–615. [CrossRef]
13. Lin, Y.-L.; Savage, L.C., III. Effects of landfall location and the approach angle of a cyclone vortex encountering a mesoscale mountain range. *J. Atmos. Sci.* **2011**, *68*, 2095–2106. [CrossRef]
14. Huang, Y.-H.; Wu, C.-C.; Wang, Y. The influence of island topography on typhoon track deflection. *Mon. Weather Rev.* **2011**, *139*, 1708–1727. [CrossRef]
15. Wu, C.-C.; Li, T.-H.; Huang, Y.-H. Influence of mesoscale topography on tropical cyclone tracks: Further examination of the channeling effect. *J. Atmos. Sci.* **2015**, *72*, 3032–3050. [CrossRef]
16. Tang, C.K.; Chan, J.C. Idealized simulations of the effect of Taiwan topography on the tracks of tropical cyclones with different sizes. *Q. J. R. Meteorol. Soc.* **2016**, *142*, 793–804. [CrossRef]
17. Tang, C.K.; Chan, J.C. Idealized simulations of the effect of Taiwan topography on the tracks of tropical cyclones with different steering flow strengths. *Q. J. R. Meteorol. Soc.* **2016**, *142*, 3211–3221. [CrossRef]
18. Huang, C.-Y.; Chen, C.-A.; Chen, S.-H.; Nolan, D.S. On the upstream track deflection of tropical cyclones past a mountain range: Idealized experiments. *J. Atmos. Sci.* **2016**, *73*, 3157–3180. [CrossRef]
19. Hsu, L.-H.; Su, S.-H.; Fovell, R.G.; Kuo, H.-C. On typhoon track deflections near the east coast of Taiwan. *Mon. Weather Rev.* **2018**, *146*, 1495–1510. [CrossRef]
20. Huang, K.-C.; Wu, C.-C. The impact of idealized terrain on upstream tropical cyclone track. *J. Atmos. Sci.* **2018**, *75*, 3887–3910. [CrossRef]
21. Huang, C.-Y.; Huang, C.-H.; Skamarock, W.C. Track deflection of Typhoon Nesat (2017) as realized by multiresolution simulations of a global model. *Mon. Weather Rev.* **2019**, *147*, 1593–1613. [CrossRef]

22. Chen, S.-Y.; Shih, C.-P.; Huang, C.-Y.; Teng, W.-H. An impact study of GNSS RO data on the prediction of Typhoon Nepartak (2016) using a multiresolution global model with 3D-hybrid data assimilation. *Weather Forecast.* **2021**, *36*, 957–977.
23. Huang, C.-Y.; Lin, J.-Y.; Skamarock, W.C.; Chen, S.-Y. Typhoon forecasts with dynamic vortex initialization using an unstructured mesh global model. *Mon. Weather Rev.* **2022**, in press. [CrossRef]
24. Huang, C.-Y.; Ruan, C.-C.; Kuo, H.-C.; Chen, J.-H. Track deflection of Typhoon Maria (2018) during a westbound passage offshore of northern Taiwan: Topographic influence. *Mon. Weather Rev.* **2020**, *148*, 4519–4544. [CrossRef]
25. Huang, C.-Y.; Sha, S.-H.; Kuo, H.-C. A modeling study of Typhoon Lekima (2019) with the topographic influence of Taiwan. *Mon. Weather Rev.* **2022**, *150*, 1993–2011. [CrossRef]
26. Huang, C.-Y.; Lin, J.-Y.; Kuo, H.-C.; Chen, D.-S.; Hong, J.-S.; Hsiao, L.-F.; Chen, S.-Y. A numerical study for Tropical Cyclone Atsani (2020) past offshore of southern Taiwan under topographic influences. *Atmosphere* **2022**, *13*, 618. [CrossRef]
27. Skamarock, W.C.; Klemp, J.B.; Duda, M.G.; Fowler, L.D.; Park, S.-H.; Ringler, T.D. A multiscale nonhydrostatic atmospheric model using centroidal Voronoi tesselations and C-grid staggering. *Mon. Weather Rev.* **2012**, *140*, 3090–3105. [CrossRef]
28. Kaplan, J.; DeMaria, M. Large-scale characteristics of rapidly intensifying tropical cyclones in the North Atlantic basin. *Weather Forecast.* **2003**, *18*, 1093–1108. [CrossRef]
29. Shi, D.; Chen, G.; Wang, K.; Bi, X.; Chen, K. Evaluation of two initialization schemes for simulating the rapid intensification of Typhoon Lekima (2019). *Adv. Atmos. Sci.* **2020**, *37*, 987–1006. [CrossRef]
30. Shi, D.; Chen, G. Double warm-core structure and potential vorticity diagnosis during the rapid intensification of Supertyphoon Lekima (2019). *J. Atmos. Sci.* **2021**, *78*, 2471–2492. [CrossRef]
31. Yang, Y.-T.; Kuo, H.-C.; Hendricks, E.A.; Peng, M.S. Structural and intensity changes of concentric eyewall typhoons in the western North Pacific basin. *Mon. Weather Rev.* **2013**, *141*, 2632–2648. [CrossRef]
32. Nguyen, T.C.; Huang, C.-Y. A comparative modeling study of Supertyphoons Mangkhut and Yutu (2018) past the Philippines with ocean-coupled HWRF. *Atmosphere* **2021**, *12*, 1055. [CrossRef]
33. Wu, L.; Wang, B. A potential vorticity tendency diagnostic approach for tropical cyclone motion. *Mon. Weather Rev.* **2000**, *128*, 1899–1911. [CrossRef]
34. Tsujino, S.; Kuo, H.-C. Potential vorticity mixing and rapid intensification in the numerically simulated Supertyphoon Haiyan (2013). *J. Atmos. Sci.* **2020**, *77*, 2067–2090. [CrossRef]
35. Wang, H.; Wang, Y. A numerical study of Typhoon Megi (2010). Part I: Rapid intensification. *Mon. Weather Rev.* **2014**, *142*, 29–48. [CrossRef]